catalysts

MDPI

Article

Electrocatalytic Treatment of Pharmaceutical Wastewater by Transition Metals Encapsulated by B, N-Doped CNTs

Ou Sha, Xifeng Lu and Pei Su *

Hebei Key Laboratory of Applied Chemistry, College of Environmental and Chemical Engineering, Yanshan University, Qinhuangdao 066004, China; shaou2013@ysu.edu.cn (O.S.); 13290148945@163.com (X.L.)
* Correspondence: sup@ysu.edu.cn

Abstract: The electrochemical advanced oxidation process is a promising technology for tackling wastewater pollution, but it suffers from poor pH adaptability and slow catalytic kinetics in a neutral and alkaline environment in a homogeneous system, as well as fast release of metal ions in a heterogeneous system. Herein, a boron- and nitrogen-codoped carbon nanotube-encapsulated transition metal (M@BN-C, M–Co, Cu) cathode with a similar structure was synthesized to explore activity trends and mechanisms. Characteristics of Co@BN-C and Cu@BN-C cathodes were examined and compared with the previously synthesized Fe@BN-C bifunctional cathode. The activity of sulfamethazine (SMT) degradation by the Co@BN-C cathode was higher than both Fe@BN-C and Cu@BN-C at pH = 3 and pH = 7, respectively. However, the activity of Co@BN-C was also higher than that of Cu@BN-C and lower than that of Fe@BN-C at pH = 9. It was observed that $^{\bullet}OH$ and $^{1}O_2$ were the main reactive oxygen species (ROS) using Co@BN-C and Cu@BN-C cathodes. The Co@BN-C generated the highest $^{\bullet}OH$ for efficient SMT degradation through abundant H_2O_2 generation, exhibiting the highest catalytic activity compared with the Cu@BN-C cathode. Overall, SMT degradation on the Co@BN-C cathode demonstrated better catalytic performance in real wastewater. This study provided insights into the fundamental catalytic trends and mechanisms of ROS production via the M@BN-C cathode, thus contributing to the development of the M@BN-C cathode for catalytic organic pollutant degradation.

Keywords: electrocatalysis; water treatment; bifunctional cathode; reactive oxygen species; mechanism

Citation: Sha, O.; Lu, X.; Su, P. Electrocatalytic Treatment of Pharmaceutical Wastewater by Transition Metals Encapsulated by B, N-Doped CNTs. *Catalysts* **2023**, *13*, 1459. https://doi.org/10.3390/catal13121459

Academic Editor: Carlo Santoro

Received: 20 October 2023
Revised: 19 November 2023
Accepted: 20 November 2023
Published: 22 November 2023

1. Introduction

The discharge of pharmaceutical wastewater was the main source of antibiotics entering environmental water bodies, causing an increase in drug resistance and affecting ecological balance [1–3]. Therefore, it was an inevitable trend to remove antibiotics from pharmaceutical wastewater via green and efficient treatment technology. Compared with conventional methods for treating antibiotics, such as adsorption, coagulation, and the activated sludge method, electro-Fenton (EF) offered unique advantages such as a fast oxidation rate, high mineralization efficiency, no secondary pollution, energy conservation, and low consumption, especially for the advanced treatment of refractory wastewater [4]. In the EF process, H_2O_2 was generated through an oxygen reduction reaction and Fe^{2+} was added as a catalyst to convert H_2O_2 into highly oxidizing $^{\bullet}OH$ (Equations (1) and (2)). However, it should be noted that the best $^{\bullet}OH$ is produced at pH = 2.8–3.5 [5,6]. In order to achieve advanced water treatment, the stability, durability, and utilization of active sites were crucial for the catalytic activity of cathodes. In response to the Fe^{2+} limitation, heterogeneous catalysts have been developed as substitutes. However, these catalysts faced challenges including poor stability, leaching of active metals, secondary pollution, and reduced activity [7,8].

$$Fe^{2+} + H_2O_2 \rightarrow Fe^{3+} + {}^{\bullet}OH + OH^{-} \quad (1)$$

$$O_2 + 2e^- + 2H^+ \rightarrow H_2O_2 \quad (2)$$

Recently, a new approach emerged in the field of EF technology, which involved the development of multifunctional cathodes with heteroatom doping, functionalization, or transition metal modification. This innovation aimed to address the drawbacks associated with the extensive use of Fe^{2+} catalysts and expand the pH applicability [9–11]. Specifically, these modified cathodes allowed for the simultaneous generation of H_2O_2 and $^{\bullet}OH$ on their surface, facilitating the easy separation and recovery of catalysts and enabling continuous operation of the treatment system. Introducing heteroatoms such as nitrogen, sulfur, and phosphorus into the carbon skeleton can alter the chemical properties of carbon materials and improve catalytic activity [12]. Although a large number of transition-metal-based catalysts have been developed to improve the yield of $^{\bullet}OH$ through Fenton-like catalysis, significant drawbacks have been noted, such as rapid release of metal ions and slow catalytic kinetics in neutral and alkaline environments [13]. However, a limitation of heteroatom-doped or functionalized carbon materials lies in their relatively low activity [14,15]. Metal-modified cathodes demonstrated high catalytic efficiency but suffered from issues such as metal leaching and strict valence requirements that hindered their practical applications [16–18]. To tackle these challenges, "nanoconfinement" has been introduced to enhance metal stability. This approach involved the immobilization and stabilization of active sites within a bifunctional cathode. By successfully overcoming the technical bottleneck associated with the loss, aggregation, and deactivation of conventional nanoparticles, wastewater purification efficiency based on confined nanoparticles has been reported to increase several times [16,19–21].

The use of nanoconfinement to achieve reactive oxygen species (ROS) transformation in electrochemical advanced oxidation processes has gained significant attention [22]. Researchers have found that encapsulating active metals within confined nano-spaces not only reduces the deactivation of active sites but also utilizes the interaction between the nano-space and surface interface to accurately control and accelerate chemical reactions [23]. For instance, when iron oxide was used as a catalyst with the cavity of carbon nanotubes (CNTs), the Fenton reaction for the degradation of methylene blue transitioned from $^{\bullet}OH$ domination to $^1O_2$ oxidation [22]. In line with this, our previous research involved the preparation of boron- and nitrogen-codoped CNTs with embedded nano-iron particles (Fe@BN-C) as a bifunctional cathode, which successfully achieved $^1O_2$ production instead of $^{\bullet}OH$ [24]. However, the catalytic mechanism of other transition metals in achieving the conversion of ROS remained unclear. There have been few studies on the bifunctional cathodes modified with metal-heteroatoms-carbon catalysts with different transition metal centers, let alone that reveal the properties of transition metals in the catalytic activity of EF and their mechanisms for different reaction species. Most metal-heteroatoms-carbon catalysts mainly produce H_2O during the $4e^-$ process and are not suitable for the in situ production of H_2O_2 as cathodes. Therefore, it is needed urgently to synthesize transition metal-heteroatoms-carbon catalysts with uniform structures and metal sites in order to fully reveal their catalytic activity and explore the reaction mechanism of reaction species formation, which is crucial for achieving efficient and low-energy-consumption pollutant removal within a wide pH range.

Herein, the Co@BN-C and Cu@BN-C bifunctional cathode was prepared. The cycling behavior of the Co@BN-C and Cu@BN-C cathode on sulfamethazine (SMT) was explored, specifically focusing on the removal of the antibiotic at different pH. The application prospect of the Co@BN-C and Cu@BN-C cathode was investigated for the removal of SMT from simulated and real wastewater. Furthermore, the mechanism of the Co@BN-C and Cu@BN-C cathode was evaluated by comparing the electrochemical analysis and electron paramagnetic resonance (EPR) of the ROS generated by $^1O_2$ and $^{\bullet}OH$. More importantly, the characteristics of the Co@BN-C and Cu@BN-C cathode were examined and compared with the previously synthesized Fe@BN-C bifunctional cathode [24].

2. Results

2.1. The Morphology of M@BN-C

The Fe@BN-C and Co@BN-C exhibited a tubular structure, similar to CNTs, as shown in the field-emission scanning electron microscopy (FESEM) images (Figure 1a,b). It was observed that the nanotube diameter of Co@BN-C was larger than that of Fe@BN-C. In contrast, Cu@BN-C has a columnar structure with shorter and coarser nanotubes (Figure 1c). High-resolution transmission electron microscopy (HRTEM) images revealed that the nano-metal particles were enclosed in the carbon cavity (Figure 1d–f). Based on our previous research [20,24], the M@BN-C structure consisted of B, N-codoped CNTs with zero-valent metal confinement. Therefore, when considering the M@BN-C materials, similarities in structure and physicochemical properties should be taken into account [25]. As shown in Figure 2, the broad diffraction peaks at 26.1° (0 0 2) are indexed to the defective structure of graphite carbon in all M@BN-C [9]. The peaks in the X-ray diffraction (XRD) pattern are indexed to zero-valence Fe (44.72°), Co (44°), and Cu (43.3°), respectively [26–28]. Overall, it suggested the structural similarity of M@BN-C.

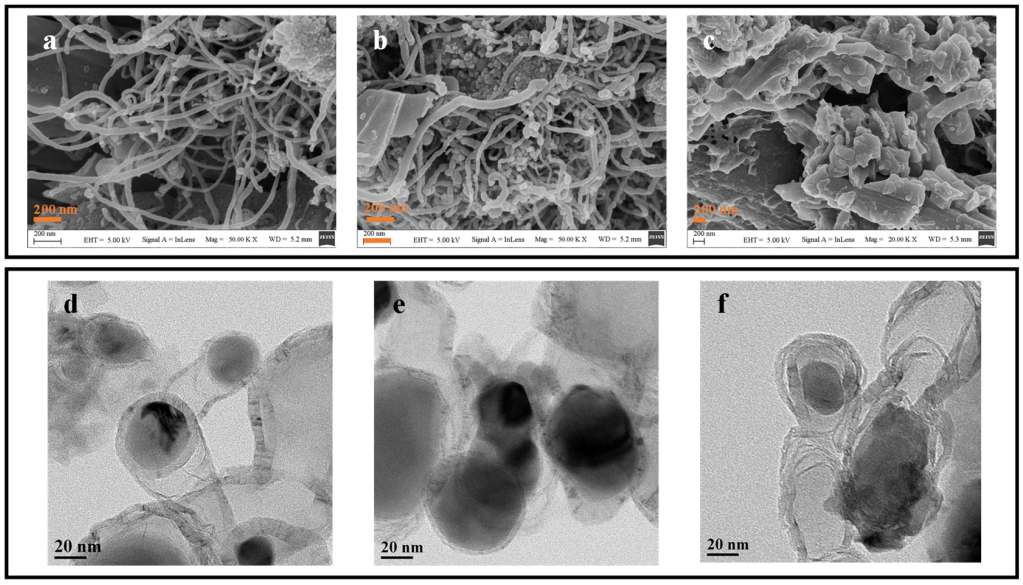

Figure 1. The FESEM images of (**a**) Fe@BN-C, (**b**), Co@BN-C, and (**c**) Cu@BN-C and the HRTEM images of (**d**) Fe@BN-C, (**e**) Co@BN-C, and (**f**) Cu@BN-C.

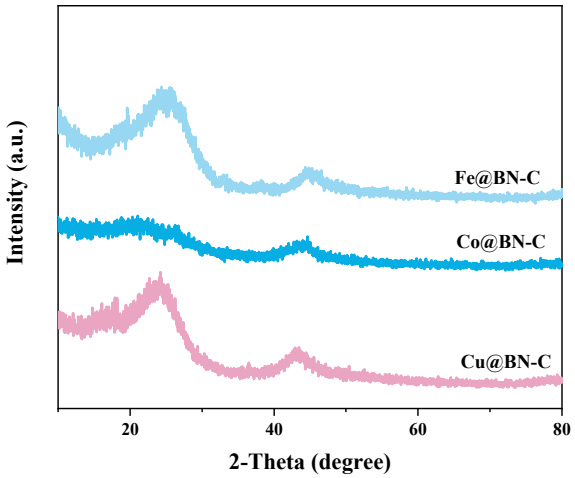

Figure 2. XRD pattern of M@BN-C catalysts.

2.2. The Catalytic Performance of M@BN-C

When the catalytic performance of bifunctional cathodes was evaluated, the SMT removal at pH = 7 was determined using M@BN-C with 3 mg cm^{-2} loading. The adsorption performance was 10.26% for the Fe@BN-C cathode, 10.70% for the Co@BN-C cathode, and 10.45% for the Cu@BN-C cathode (Figure 3a). This indicated that the adsorption was not a dominant role in SMT removal. It is observed from Figure 3a that Co@BN-C achieved 100% SMT removal within 120 min, exhibiting superior performance compared with the Co@BN-C and Cu@BN-C cathodes. The Fe@BN-C and Cu@BN-C cathodes achieved SMT removal of 92.13% and 73.62% within 120 min, respectively. Therefore, the pseudo-first-order rate constant (*k*) [29] for SMT removal on the Co@BN-C cathode was determined to be 0.039 min^{-1}, which was 1.77-fold that of the *k* on the Fe@BN-C cathode (0.022 min^{-1}) and 3.55-fold that of the *k* on the Cu@BN-C cathode (0.011 min^{-1}), as shown in Figure 3b.

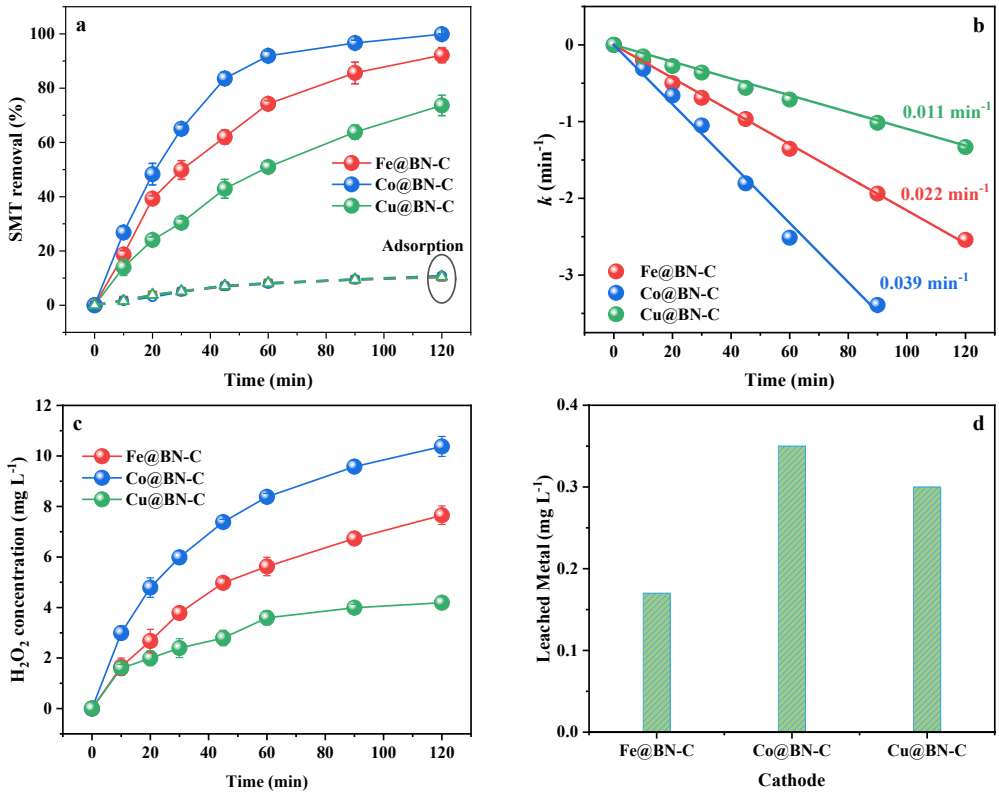

Figure 3. (**a**) The SMT degradation and adsorption by M@BN-C cathode; (**b**) the kinetics analysis as a pseudo-first-order reaction for SMT degradation by M@BN-C cathode; (**c**) the H_2O_2 concentration and (**d**) leaching metal concentration by M@BN-C cathode at 120 min. Experiment condition: cathode potential: −0.8 V (vs. saturated calomel electrode (SCE)); catalysts loading: 3 mg cm^{-2}; V: 50 mL; V_{air}: 0.4 L min^{-1}; SMT concentration: 10 mg L^{-1}; pH = 7.

The difference in the catalytic performance of the M@BN-C cathode was assessed by evaluating the generated H_2O_2 concentration and leached metal concentration. The concentration of H_2O_2 production was found to be consistent with the trend of SMT removal, as shown in Figure 3a,c. It was observed that the H_2O_2 yield on the Co@BN-C cathode was 10.38 mg L^{-1} at 120 min, which was 1.36-fold and 2.48-fold that of the Fe@BN-C and the Cu@BN-C cathode, respectively. This finding was supported by previous studies on metal-nitrogen-carbon single-atom catalysts for H_2O_2 production [30]. It could be inferred that the superior performance of the Co@BN-C cathode could be attributed to its higher H_2O_2 yield, which served as a precursor of generated ROS for pollutant degradation [31]. On the other hand, the leached concentration of Co, Fe, and Cu from the M@BN-C cathode was found to be 0.35 mg L^{-1}, 0.17 mg L^{-1}, and 0.3 mg L^{-1}, respectively

(Figure 3d). The higher leaching metal would lead to chemical reactions occurring in the electrolyte instead of the cathode surface, resulting in ROS generation [32,33]. In addition, the presence of higher metal concentrations could also contribute to the formation of metal sludge, causing secondary pollution [6,34].

When the M@BN-C cathode was used, the SMT was mineralized to generate intermediates by ROS oxidation. The total organic carbon (TOC) removal reached 60.00% within 120 min by the Co@BN-C cathode, which was higher than Fe@BN-C (39.43%) and Cu@BN-C (33.33%) (Figure 4a). The MCE of SMT removal after 120 min is exhibited in Figure 4b. The mineralization current efficiency (MCE) of the Fe@BN-C, Co@BN-C, and Cu@BN-C cathodes was 57.25%, 38.71%, and 80.65%, respectively (Figure 4b). Therefore, the Co@BN-C cathode might produce more ROS or different intermediates resulting in varying TOC removal. The effect of different ROS generation on mineralization by M@BN-C cathode is discussed in the following content.

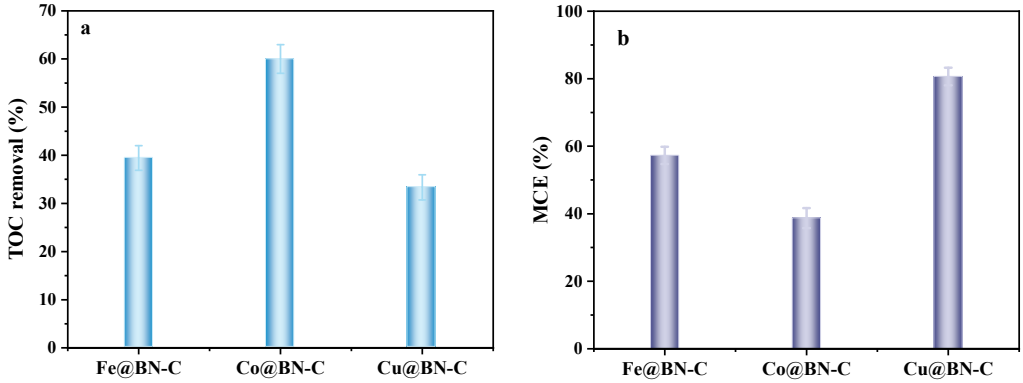

Figure 4. (**a**) TOC removal (blue) and (**b**) MCE (purple) by M@BN-C cathode for SMT removal at 120 min. Experiment condition: cathode potential: −0.8 V (vs. SCE); catalysts loading: 3 mg cm^{-2}; V: 50 mL; V_{air}: 0.4 L min^{-1}; SMT concentration: 10 mg L^{-1}; pH = 7.

2.3. Catalytic Mechanism of M@BN-C Cathode

The difference in the electrochemical performance of the M@BN-C cathode was evaluated. It was observed that the onset potential and limiting current density of the Co@BN-C cathode were better than those of the Fe@BN-C cathode (Figure 5a), indicating faster electron transfer on the Co@BN-C cathode. Moreover, the limiting current density of the Fe@BN-C cathode was higher than that of the Cu@BN-C cathode. The order of current density was consistent with the removal of SMT by the M@BN-C cathode. From the Nyquist plot analysis, the ohmic resistance (R_0), charge transfer resistance (R_{ct}), and diffusion resistance (R_d) were determined (Figure 5b). The R_0 values of the M@BN-C cathode showed no significant differences (25.78 Ω for Fe@BN-C, 27.07 Ω for Co@BN-C, 27.45 Ω for Cu@BN-C). The R_{ct} values for Fe@BN-C, Co@BN-C, and Cu@BN-C were 23.79 Ω, 15.31 Ω, and 43.84 Ω, respectively. This suggested that electron transfer was accelerated following the order of Co, Fe, and Cu, which was consistent with the literature [30]. The corrosion potential, obtained from the polarization curve analysis (Figure 5c), was used to evaluate the leaching rate of the transition metal. The corrosion potential observed was −0.19 V for Co@BN-C, −0.13 V for Cu@BN-C, and −0.067 V (vs. SCE) for Fe@BN-C. These results confirmed that Co facilitated charge transfer, which aligned with the leaching of transition metal (Figure 3d).

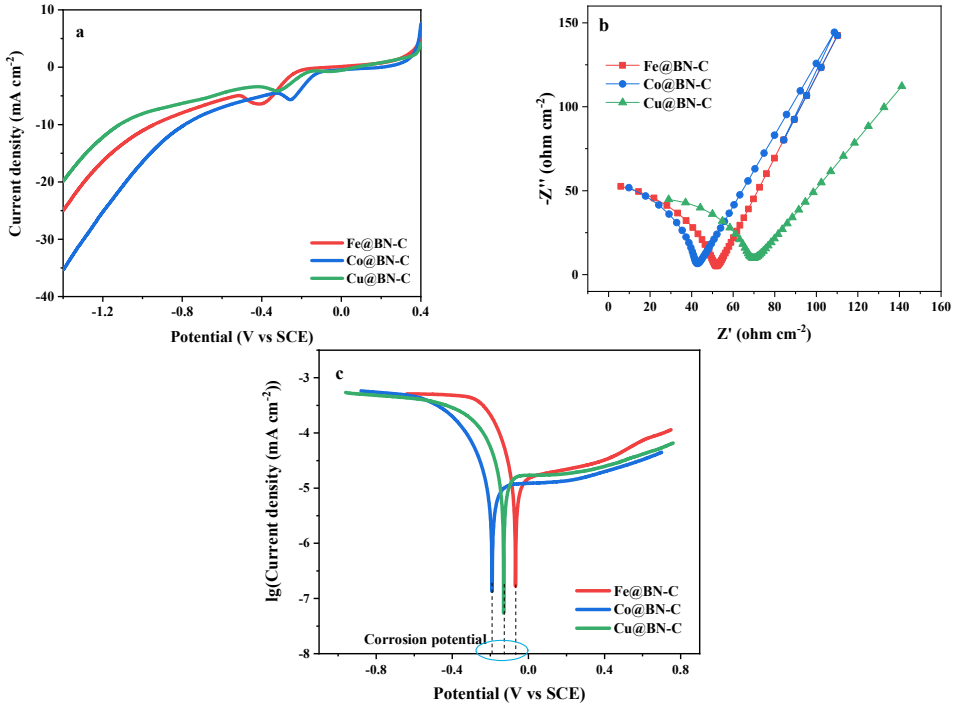

Figure 5. (**a**) The linear sweep voltammetry (LSV) curve, (**b**) the Nyquist plot, and (**c**) the polarization curve of the M@BN-C cathode (The blue circle represents the corrosion potential).

The generation of ROS was determined via EPR spectra in order to explore the reaction mechanism of the M@BN-C cathode. Figure 6a,c show the characteristic peak of 2,2,6,6-Tetramethylpiperidine (TEMP)-$^1O_2$, which was obtained when TEMP was added to quench $^1O_2$. These peaks were identical to the 1:1:1 peaks [35,36]. The intensity of the TEMP-$^1O_2$ peak was found to increase with the catalytic reaction on the M@BN-C cathode. Among the M@BN-C cathodes, the Fe@BN-C cathode exhibited the highest production of $^1O_2$, reaching 23.09 times that of 0 min (Figure 6a). The Co@BN-C and Cu@BN-C cathodes also showed significant increases in $^1O_2$ generation, with intensities of 5.52 and 2.69 times that of TEMP alone, respectively. The generation of $^{\bullet}$OH, characterized using 5,5-dimethyl-1-pyrroline N-oxide (DMPO), showed a characteristic peak of DMPO-$^{\bullet}$OH on the Co@BN-C and Cu@BN-C cathodes (Figure 6d,e), presenting a 1:2:2:1 peak [32,37]. However, no $^{\bullet}$OH generation was observed on the Fe@BN-C cathode, mainly due to the conversion of all generated H_2O_2 into $^1O_2$ in the presence of $O_2^{\bullet-}$/$HO_2^{\bullet-}$ [38]. The catalytic process of $^1O_2$ was expressed by Equations (3)–(5) (*OH represented surface-bound $^{\bullet}$OH), and the $^{\bullet}$OH was identified as an intermediate, mainly involved in the $^1O_2$ production by surface-bound $^{\bullet}$OH conversion. Similar generation processes of $^1O_2$ were observed, whereas $^{\bullet}$OH generation was detected only on the Co@BN-C and Cu@BN-C cathodes, indicating a more homogeneous catalytic process due to higher Co and Cu leaching in the solution. The different ROS yields resulted in variations in pollutant degradation and mineralization efficiencies. Because $^{\bullet}$OH has higher oxidation potential compared with $^1O_2$ [39], the Co@BN-C cathode exhibited the highest degradation efficiency of SMT. The aniline moiety of SMT was more readily oxidized to form nitrobenzene in the presence of $^1O_2$ compared with $^{\bullet}$OH [40–42], resulting in lower TOC removal by the Fe@BN-C cathode.

$$Fe^{3+} + H_2O_2 \rightarrow O_2^{\bullet-} + 2H^+ + Fe^{2+} \quad (3)$$

$$Fe^{2+} + H_2O_2 \rightarrow {}^*OH + OH^- + Fe^{3+} \quad (4)$$

$$HO_2^{\bullet-} + {}^*OH \rightarrow H_2O + {}^1O_2 \quad (5)$$

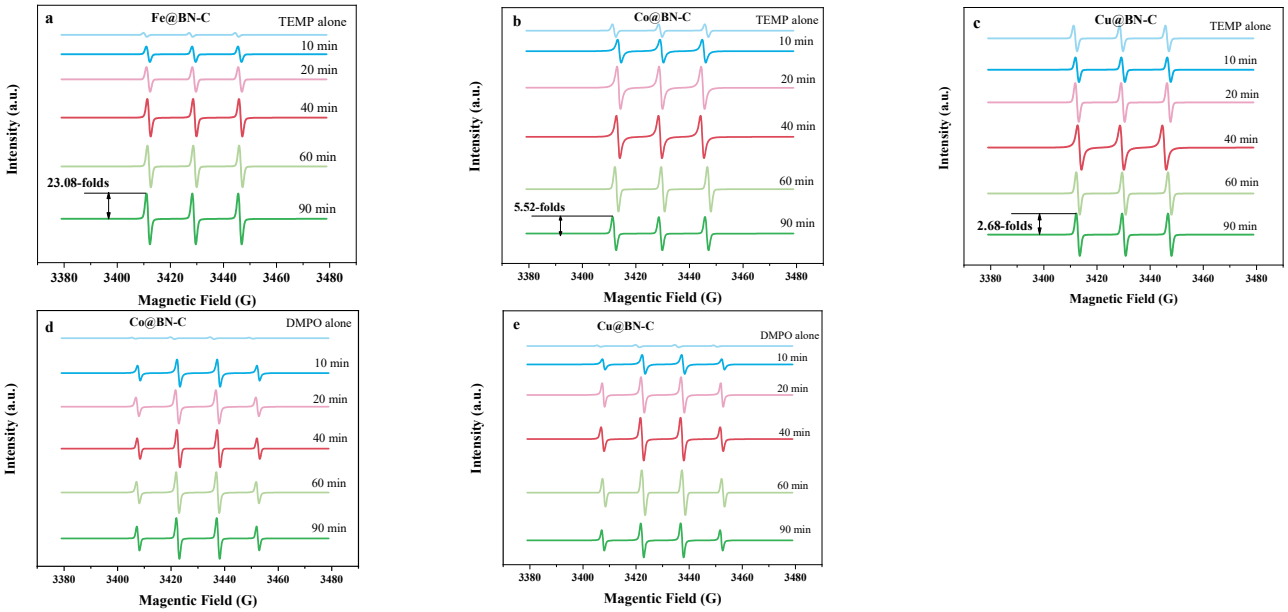

Figure 6. EPR spectra of $^1O_2$ by (**a**) Fe@BN-C, (**b**) Co@BN-C, and (**c**) Cu@BN-C cathodes. EPR spectra of •OH by (**d**) Co@BN-C and (**e**) Cu@BN-C cathodes. Experiment condition: cathode potential: −0.8 V (vs. SCE); catalysts loading: 3 mg cm^{-2}; V: 50 mL; V_{air}: 0.4 L min^{-1}; DMPO: 100 mM; TEMP: 100 mM; pH = 7.

2.4. The Effect of pH on Catalytic Performance by M@BN-C

To evaluate the oxidation ability of ROS and the potential application of M@BN-C, the effect of pH on the performance of the M@BN-C cathode was investigated. The SMT removal by the M@BN-C cathode was measured at different pH conditions, and it was observed that the SMT removal decreased as the pH increased (Figure 7a–c). This decline could be attributed to the favorable production of •OH under acidic conditions, which facilitated pollutant degradation [43,44]. In addition, higher leaching of transition metal resulted in the generation of more free •OH and less $^1O_2$. Notably, the Fe@BN-C cathode exhibited consistent SMT removal at pH = 9 (90.14%) compared with (92.13%), suggesting a wider application range of the $^1O_2$ at pH = 9. This characteristic presented a significant advantage of traditional EF technology in treating neutral and alkaline wastewater. Conversely, for the Co@BN-C and Cu@BN-C cathodes (Figure 7b,c), the SMT removal at pH = 9 significantly decreased compared with pH = 3 due to the decreased oxidation ability of •OH at lower pH. The *k* value for SMT removal was calculated, and it was found that the *k* value for the Co@BN-C cathode at pH = 3 (0.10 min^{-1}) was 2.36-fold that of Fe@BN-C and 6.23-fold that of Cu@BN-C, respectively (Figure 7d). However, the *k* value for the Co@BN-C cathode at pH = 9 was only 85% of Fe@BN-C and 1.99-fold that of Cu@BN-C. Consequently, the Co@BN-C cathode was more suitable for acidic and neutral conditions in pollutant removal, while the Fe@BN-C cathode demonstrated greater potential for wastewater purification in alkaline environments.

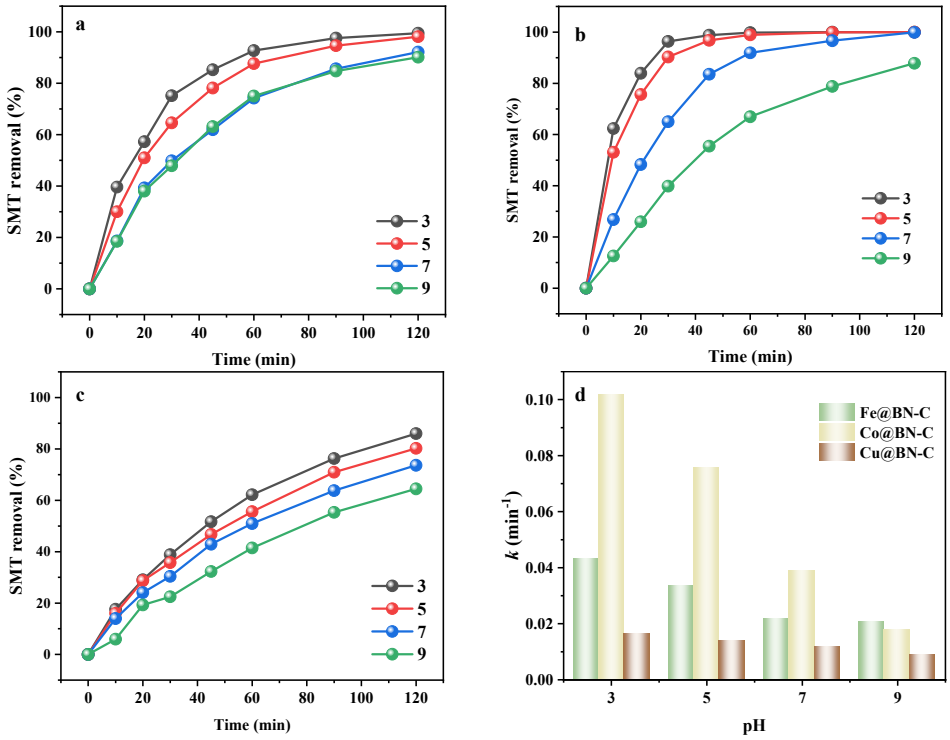

Figure 7. The effect of pH on the SMT degradation by (**a**) Fe@BN-C, (**b**) Co@BN-C, and (**c**) Cu@BN-C cathodes. (**d**) The *k* of SMT removal by Fe@BN-C, Co@BN-C, and Cu@BN-C cathodes at different pH. Experiment condition: cathode potential: −0.8 V (vs. SCE); catalysts loading: 3 mg cm^{-2}; V: 50 mL; V_{air}: 0.4 L min^{-1}.

2.5. Cycling Performance of the M@BN-C Cathode

The stability of the M@BN-C cathode was further evaluated in the electrocatalytic process to assess its potential application. It was observed that the removal efficiency of SMT gradually decreased from 92.13% in the first cycle of Fe@BN-C to 87.17% in the fifth cycle (Figure 8a). This indicated that the Fe@BN-C cathode maintained good stability, primarily due to the low leaching of Fe and the high stability of $^1O_2$ [36,45]. In contrast, the Co@BN-C cathode exhibited better catalytic performance than the Fe@BN-C cathode (Figure 3a), but the SMT degradation was only 76.23% after the fifth cycle (Figure 8b). This was mainly attributed to the significant leaching of Co during each catalytic process, resulting in a decrease in the yield of •OH. In contrast, the decline in catalytic performance of the Cu@BN-C cathode was not significant due to the limited production of •OH and $^1O_2$ (Figure 8c). Overall, the *k* values for SMT removal by M@BN-C cathodes are shown in Figure 8d. After five cycles, the *k* values for the Fe@BN-C, Co@BN-C, and Cu@BN-C cathodes decreased by 19.91%, 68.99%, and 27.19%, respectively. These findings highlighted that the Fe@BN-C cathode was conducive to stable wastewater purification, leading to reduced cathode costs.

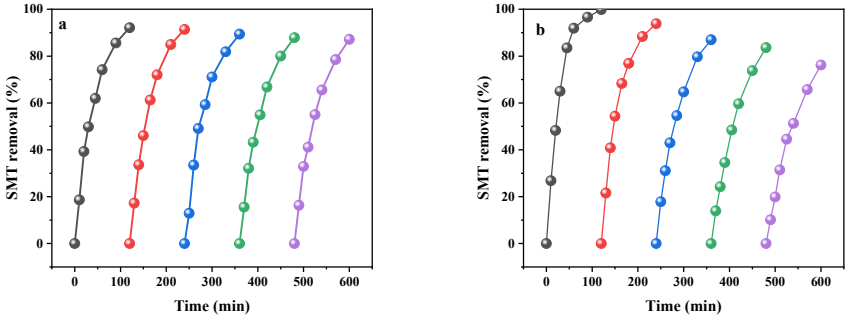

Figure 8. *Cont.*

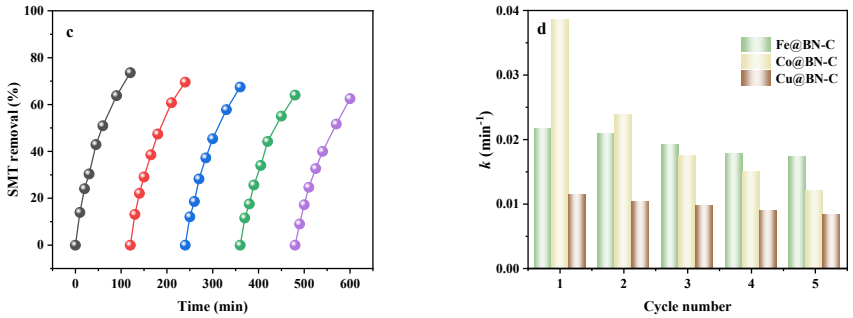

Figure 8. Recyclability of the (**a**) Fe@BN-C, (**b**) Co@BN-C, and (**c**) Cu@BN-C cathodes for SMT degradation and (**d**) *k* value. Experiment condition: cathode potential: −0.8 V (vs. SCE); catalysts loading: 3 mg cm^{-2}; V: 50 mL; V_{air}: 0.4 L min^{-1}; pH = 7.

2.6. Application Prospect of the M@BN-C Cathode

In generally, there are abundant inorganic ions and natural organic macromolecules in actual wastewater. The effects of the presence of humic acid (HA), HCO_3^-, Cl^-, and NO_3^- on the degradation of SMT by M@BN-C cathode were evaluated. The addition of HCO_3^- could regulate the pH of the electrolyte in an alkaline environment [34]. Since the Fe@BN-C cathode does not produce •OH, the presence of HA, HCO_3^-, Cl^-, and NO_3^- had no significant effect on the degradation of SMT by the Fe@BN-C cathode (Figure 9a). The degradation of SMT slightly decreased from 92.13% to 90.47% by the Fe@BN-C cathode. The SMT degradation decreased from 99.88% to 45.29% and from 73.62% to 40.54%, respectively, due to the presence of HCO_3^-, which can quench •OH [44]. Compared with traditional EF dominated by •OH, the $^1O_2$ dominant electrocatalytic process had more advantages in the effect of coexisting impurities. It has been reported that the presence of HA would consume •OH instead of $^1O_2$. In addition, HA can chelate Fe^{3+} to prevent Fe^{3+} from precipitation under neutral conditions, thereby promoting the corrosion of Fe^0 [46]. Therefore, the addition of HA will not affect the SMT degradation by the Fe@BN-C cathode in the electrocatalytic process, and the decline of SMT removal was observed by the Cu@BN-C and Co@BN-C cathodes in the presence of HA.

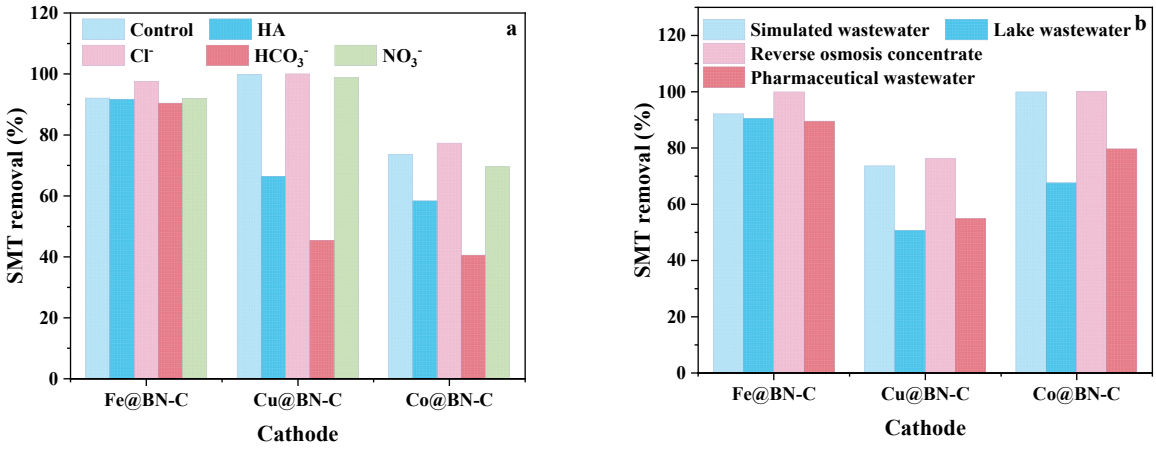

Figure 9. (**a**) Effect of background constituents (Cl^-, HCO_3^- and NO_3^-: 10 mM; HA: 10 mg L^{-1}); (**b**) SMT degradation in the simulated wastewater, lake water, reverse osmosis concentrate, and pharmaceutical wastewater in electrocatalytic process of M@BN-C cathode. Experiment condition: cathode potential: −0.8 V (vs. SCE); catalysts loading: 3 mg cm^{-2}; V: 50 mL; V_{air}: 0.4 L min^{-1}; pH = 7.

In order to further evaluate the application potential of the M@BN-C cathode in real matrices, it was conducted in lake water, reverse osmosis concentrated water, and pharmaceutical wastewater. The quality parameters of water/wastewater are shown

in Table 1. As shown in Figure 9b, the Fe@BN-C cathode is not affected by SMT in all real matrices. The Co@BN-C and Cu@BN-C cathodes only reached low SMT removal in lake water and pharmaceutical wastewater, mainly due to the interference of coexisting substances in the wastewater caused by $^{\bullet}OH$ generation. In addition, SMT degradation achieved faster kinetics by the M@BN-C cathode in reverse osmosis concentrated water, mainly because the concentration of reverse osmosis concentrated water (3384.4 mg L^{-1}) was much higher than that of other water. The high content of ROS reacts with ROS and produces reactive chlorine (such as Cl_2 and HOCl) [47], accelerating the removal process of pollutants. Therefore, the M@BN-C cathode has the advantage for application prospects, especially in treating high salinity water surfaces.

Table 1. The quality parameters of the secondary wastewater effluent.

	Mati Lake	Reverse Osmosis Concentrate	Pharmaceutical Wastewater
pH	8.0	8.3	7.8
Conductivity (μS cm^{-1})	1198	4879	184.3
COD (mg L^{-1})	104.4	127.4	148.3
TOC (mg L^{-1})	32.0	509.1	40.3
Cl^- (mg L^{-1})	115.2	3384.4	40.9
HCO_3^- (mg L^{-1})	44.9	492.4	-
NO_3^- (mg L^{-1})	54.8	-	5.8

3. Materials and Methods

3.1. Chemicals and Materials

The commercially hydrophobic carbon cloth (HCP330P) was purchased from Shanghai Hesen Electric Co., Ltd, Shanghai, China. Ferric nitrate ($Fe(NO_3)_3 \cdot 9H_2O$, analytical reagent), cobalt nitrate ($Co(NO_3)_2 \cdot 6H_2O$, analytical reagent), and copper nitrate ($Cu(NO_3)_2 \cdot 3H_2O$, analytical reagent) were purchased from Tianjin Bohua Chemical Reagent Co., Ltd, Tianjin, China. Nafion solution (5 wt%) was purchased from Sigma-Aldrich (Shanghai, China) Trading Co., Ltd, China. SMT ($C_{10}H_9ClN_4O_2S$, 99%), sodium sulfate (Na_2SO_4, analytical reagent), DMPO (97%), melamine ($C_3H_6N_6$, 99%), boric acid (H_3BO_3, greater than 99.5%), and sodium chloride (NaCl, 99.5%), sodium bicarbonate ($NaHCO_3$, 99.8%), sodium nitrate ($NaNO_3$, 99%), and HA were purchased from Shanghai Aladdin Chemistry Co., Ltd., Shanghai, China. TEMP was purchased from Tianjin Sinos Opto Technology Co., Ltd, Tianjin, China.

3.2. Synthesis of Bifunctional Cathodes

The M@BN-C was prepared according to our previous research [24]. An amount of 0.06 mol of boric acid and 0.03 mol of melamine were dissolved in 300 mL of deionized water heated to 85 °C, and the solution was evenly stirred. Then, 1 mmol of $M(NO_3)_3 \cdot yH_2O$ ($Fe(NO_3)_3 \cdot 9H_2O$, $Co(NO_3)_2 \cdot 6H_2O$, and $Cu(NO_3)_2 \cdot 3H_2O$) were added to the solution and stirred for 4 h at 85 °C. Subsequently, the mixed solution was heated to 115 °C and evaporated, resulting in precipitates. The precipitates were then placed in a bake-out furnace at 80 °C. The obtained mixture was calcined at a heating rate of 2.5 °C min^{-1} to 800 °C for 3 h. The precipitates were annealed in Ar atmosphere, resulting in the formation of the catalysts, which were named M@BN-C. The characterization of Fe@BN-C was reported in our previous research [24], showing similar structure and physicochemical properties to the prepared M@BN-C [20].

To prepare the M@BN-C bifunctional cathode, the obtained M@BN-C was mixed with 0.5 mL ethanol and 0.05 mL Nafion solution (5 wt%) and ultrasonically dispersed for 10 min. The resulting ink was uniformly coated on a 7 cm^2 carbon cloth. The loading of the cathode on the carbon cloth substrate was 3 mg cm^{-2}.

3.3. Experimental Procedure

The three-electrode system was employed during SMT removal. M@BN-C, dimensionally stable anode, and SCE were used as cathode, anode, and reference electrode. The 0.5 M Na_2SO_4 containing 10 mg L^{-1} SMT with a volume of 50 mL was used as electrolyte. The pH of the electrolyte was adjusted using 0.1 M H_2SO_4 or NaOH solution. The cathode potential was set at −0.8 V (vs. SCE) and air flow rate was 0.4 L min^{-1}. The anti-interference ability of M@BN-C cathode for inorganic ions and natural organic macromolecules was evaluated when 10 mM of Cl^-, $HCO_3{}^-$, and $NO_3{}^-$ and 10 mg L^{-1} of HA were added into electrolyte.

3.4. Electrochemical Analysis

The electrochemical analysis was carried out using a three-electrode system with a CHI 760E potentiostat (CH Instruments, Chenhua, Shanghai, China). The working electrode (M@BN-C), counter electrode (platinum sheet), and SCE were utilized. LSV was conducted at a scan rate of 10 mV s^{-1} with a potential interval of −1.4 V to 0.4 V. After the open circuit potential, electrochemical impedance spectroscopy was performed in the frequency range of 0.01 Hz to 100 Hz to determine the R_0, R_{ct}, and R_d. In addition, polarization curves were measured by varying the potential from −1.1 V to 0.9 V to compare the leached rate of transition metal.

3.5. Characterization and Analytical Methods

The morphologies of the M@BN-C were characterized using FESEM (LEO-1530VP) and HRTEM (JEM-2100f). XRD (Philips-12045 B/3 diffractometer) was performed to evaluate the structure of M@BN-C.

The generated H_2O_2 concentration was measured by potassium oxalate-spectrophotometric method at 400 nm [48]. The mixture of 0.5 mL samples, 0.5 mL H_2SO_4 solution (3 M), and 0.5 mL potassium titanium (IV) oxalate solution (0.05 mol L^{-1}) was measured with UV-Vis spectrophotometer (UV759). The leaching metal from M@BN-C cathode was evaluated by the inductively coupled plasma optical emission spectrometer (ICP-OES, Thermo Elemental IRIS Intrepid II XSP). The experiments of M@BN-C cathode were both conducted three times, and the final result was taken as the average of three times the experiments. The conductivity of real wastewater in Table 1 was measured using electric conductometer (Thundermagnetic DDS-307A, Shanghai, China). EPR spectra for $^{\bullet}OH$ and $^1O_2$ were measured using a Bruker EMX Nano (Berlin, Germany) by employing the reagent 100 mM DMPO and 10 mM TEMP. The SMT concentration was evaluated by high-performance liquid chromatograph (HPLC, Ultimate 3000, ThermoFisher, Waltham, MA, USA) equipped with C18 column (3 μm, ϕ3.0 × 100 mm) at 270 nm. The mobile phase was acetonitrile: water of 35:65. TOC was measured by a TOC analyzer (Analytikjena, multi N/C 3100). The MCE (%) was calculated as follows [49]:

$$\mathrm{MCE}(\%) = \frac{\mathrm{n}FV\Delta(\mathrm{TOC})_{\mathrm{exp}}}{4.32 \times 10^7 mIt} \times 100 \quad (6)$$

where n is the electrons consumed per SMT molecule during its mineralization and was taken as 52, F is the Faraday constant (96,486 C mol^{-1}), V is the bulk volume (L), $\Delta(TOC)_{exp}$ is the TOC decay (mg L^{-1}), 4.32×10^7 is the conversion factor (3600 s h^{-1} × 12,000 mg C mol^{-1}), m represents the number of carbon atoms of SMT (12), and I and t represent current (A) and time (h), respectively.

4. Conclusions

The Co@BN-C and Cu@BN-C cathodes with similar morphological structures were prepared. Characteristics of the Co@BN-C and Cu@BN-C cathodes were compared with the previously synthesized Fe@BN-C bifunctional cathode. The activity order of pollutant removal and mineralization, as well as leaching metal, was found to be Co@BN-C > Fe@BN-C > Cu@BN-C at neutral pH when M@BN-C was used as a bifunctional cathode in the electrocatalytic process. The performance of M@BN-C cathodes was determined by

the H_2O_2 production to generate the different ROS. On the Fe@BN-C cathode, $^1O_2$ was only dominant for pollutant removal. However, on the Co@BN-C and Cu@BN-C cathodes, both $^{\bullet}OH$ and $^1O_2$ were simultaneously generated, with Co@BN-C exhibiting a higher yield than Cu@BN-C. The Co@BN-C cathode showed superiority in an acidic environment compared with the Cu@BN-C and Fe@BN-C cathodes. Due to the generation of $^{\bullet}OH$, the electrochemical process based on the Co@BN-C and Cu@BN-C cathodes declined, which was affected by background substances (HA and HCO_3^-). In conclusion, this study provided new guidance for the performance evaluation of Co@BN-C and Cu@BN-C cathodes and selecting M@BN-C for various pollutant degradation based on different ROS formations.

Author Contributions: O.S.: conceptualization, formal analysis, writing—original draft. X.L.: investigation, data curation. P.S.: conceptualization, supervision, funding acquisition, resources, writing—review and editing. All authors have read and agreed to the published version of the manuscript.

Funding: This work was financially supported by the National Natural Science Foundation of China (no. 22302170).

Data Availability Statement: Data are contained within the article.

Conflicts of Interest: The authors declare no conflict of interest or other interests that might be perceived to influence the results and/or discussion reported in this paper.

References

1. Phoon, B.L.; Ong, C.C.; Saheed, M.S.M.; Show, P.-L.; Chang, J.-S.; Ling, T.C.; Lam, S.S.; Juan, J.C. Conventional and emerging technologies for removal of antibiotics from wastewater. *J. Hazard. Mater.* **2020**, *400*, 122961. [CrossRef] [PubMed]
2. Yang, L.; Jiao, Y.; Xu, X.; Pan, Y.; Su, C.; Duan, X.; Sun, H.; Liu, S.; Wang, S.; Shao, Z. Superstructures with atomic-level arranged perovskite and oxide layers for advanced oxidation with an enhanced non-free radical pathway. *ACS Sustain. Chem. Eng.* **2022**, *10*, 1899–1909. [CrossRef]
3. Xu, X.; Zhong, Y.; Shao, Z. Double perovskites in catalysis, electrocatalysis, and photo(electro)catalysis. *Trends Chem.* **2019**, *1*, 410–424. [CrossRef]
4. Da Silva, S.W.; Welter, J.B.; Albornoz, L.L.; Heberle, A.N.A.; Ferreira, J.Z.; Bernardes, A.M. Advanced electrochemical oxidation processes in the treatment of pharmaceutical containing water and wastewater: A Review. *Curr. Pollut. Rep.* **2021**, *7*, 146–159. [CrossRef]
5. Nidheesh, P.V.; Gandhimathi, R. Trends in electro-Fenton process for water and wastewater treatment: An overview. *Desalination* **2012**, *299*, 1–15. [CrossRef]
6. Barhoumi, N.; Oturan, N.; Ammar, S.; Gadri, A.; Oturan, M.A.; Brillas, E. Enhanced degradation of the antibiotic tetracycline by heterogeneous electro-Fenton with pyrite catalysis. *Environ. Chem. Lett.* **2017**, *15*, 689–693. [CrossRef]
7. Pei, D.-N.; Liu, C.; Zhang, A.-Y.; Pan, X.-Q.; Yu, H.-Q. In situ organic Fenton-like catalysis triggered by anodic polymeric intermediates for electrochemical water purification. *Proc. Natl. Acad. Sci. USA* **2020**, *117*, 30966–30972. [CrossRef]
8. Du, X.; Wang, S.; Ye, F.; Qingrui, Z. Derivatives of metal-organic frameworks for heterogeneous Fenton-like processes: From preparation to performance and mechanisms in wastewater purification—A mini review. *Environ. Res.* **2022**, *206*, 112414. [CrossRef]
9. Ganiyu, S.O.; Huong Le, T.X.; Bechelany, M.; Esposito, G.; van Hullebusch, E.D.; Oturan, M.A.; Cretin, M. A hierarchical CoFe-layered double hydroxide modified carbon-felt cathode for heterogeneous electro-Fenton process. *J. Mater. Chem. A* **2017**, *5*, 3655–3666. [CrossRef]
10. Wang, Y.; Zhao, G.; Chai, S.; Zhao, H.; Wang, Y. Three-dimensional homogeneous ferrite-carbon aerogel: One pot fabrication and enhanced electro-Fenton reactivity. *ACS Appl. Mater. Interfaces* **2013**, *5*, 842–852. [CrossRef]
11. Chen, W.; Yang, X.; Huang, J.; Zhu, Y.; Zhou, Y.; Yao, Y.; Li, C. Iron oxide containing graphene/carbon nanotube based carbon aerogel as an efficient E-Fenton cathode for the degradation of methyl blue. *Electrochim. Acta* **2016**, *200*, 75–83. [CrossRef]
12. Ri, K.C.; Pak, S.S.; Sun, D.; Zhong, Q.; Yang, S.; Sin, S.I.; Wu, L.; Sun, Y.; Cao, H.; Han, C.; et al. Boron-doped rGO electrocatalyst for high effective generation of hydrogen peroxide: Mechanism and effect of oxygen-enriched air. *App. Catal. B: Environ.* **2024**, *343*, 123471. [CrossRef]
13. Divyapriya, G.; Srinivasan, R.; Nambi, I.M.; Senthilnathan, J. Highly active and stable ferrocene functionalized graphene encapsulated carbon felt array—A novel rotating disc electrode for electro-Fenton oxidation of pharmaceutical compounds. *Electrochim. Acta* **2018**, *283*, 858–870. [CrossRef]
14. Su, P.; Zhou, M.; Lu, X.; Yang, W.; Ren, G.; Cai, J. Electrochemical catalytic mechanism of N-doped graphene for enhanced H_2O_2 yield and in-situ degradation of organic pollutant. *Appl. Catal. B Environ.* **2019**, *245*, 583–595. [CrossRef]

15. Wu, P.; Zhang, Y.; Chen, Z.; Duan, Y.; Lai, Y.; Fang, Q.; Wang, F.; Li, S. Performance of boron-doped graphene aerogel modified gas diffusion electrode for in-situ metal-free electrochemical advanced oxidation of Bisphenol A. *Appl. Catal. B Environ.* **2019**, *255*, 117784. [CrossRef]
16. Su, P.; Zhou, M.; Ren, G.; Lu, X.; Du, X.; Song, G. A carbon nanotube-confined iron modified cathode with prominent stability and activity for heterogeneous electro-Fenton reactions. *J. Mater. Chem. A* **2019**, *7*, 24408–24419. [CrossRef]
17. Zhao, H.; Qian, L.; Chen, Y.; Wang, Q.; Zhao, G. Selective catalytic two-electron O_2 reduction for onsite efficient oxidation reaction in heterogeneous electro-Fenton process. *Chem. Eng. J.* **2018**, *332*, 486–498. [CrossRef]
18. Zhao, H.; Wang, Q.; Chen, Y.; Tian, Q.; Zhao, G. Efficient removal of dimethyl phthalate with activated iron-doped carbon aerogel through an integrated adsorption and electro-Fenton oxidation process. *Carbon* **2017**, *124*, 111–122. [CrossRef]
19. Xiao, F.; Wang, Z.; Fan, J.; Majima, T.; Zhao, H.; Zhao, G. Selective electrocatalytic reduction of oxygen to hydroxyl radicals via 3-electron pathway with FeCo alloy encapsulated carbon aerogel for fast and complete removing pollutants. *Angew. Chem. Int. Edit.* **2021**, *60*, 10375–10383. [CrossRef]
20. Su, P.; Fu, W.; Hu, Z.; Jing, J.; Zhou, M. Insights into transition metal encapsulated N-doped CNTs cathode for self-sufficient electrocatalytic degradation. *Appl. Catal. B Environ.* **2022**, *313*, 121457. [CrossRef]
21. Yang, Z.; Qian, J.; Yu, A.; Pan, B. Singlet oxygen mediated iron-based Fenton-like catalysis under nanoconfinement. *Proc. Natl. Acad. Sci. USA* **2019**, *116*, 6659–6664. [CrossRef] [PubMed]
22. Zhao, H.; Qian, L.; Guan, X.; Wu, D.; Zhao, G. Continuous bulk FeCuC aerogel with ultradispersed metal nanoparticles: An efficient 3D heterogeneous electro-Fenton cathode over a wide range of pH 3−9. *Environ. Sci. Technol.* **2016**, *50*, 5225–5233. [CrossRef] [PubMed]
23. Koblenz, T.S.; Wassenaar, J.; Reek, J.N.H. Reactivity within a confined self-assembled nanospace. *Chem. Soc. Rev.* **2008**, *37*, 247–262. [CrossRef] [PubMed]
24. Su, P.; Fu, W.; Du, X.; Guo, J.; Zhou, M. Cost-effective degradation of pollutants by in-situ electrocatalytic process on Fe@BN-C bifunctional cathode: Formation of $^1O_2$ with high selectivity under nanoconfinement. *Chem. Eng. J.* **2023**, *452*, 139693. [CrossRef]
25. Gao, Y.; Wu, T.; Yang, C.; Ma, C.; Zhao, Z.; Wu, Z.; Cao, S.; Geng, W.; Wang, Y.; Yao, Y.; et al. Activity trends and mechanisms in peroxymonosulfate-assisted catalytic production of singlet oxygen over atomic metal-N-C catalysts. *Angew. Chem. Int. Ed.* **2021**, *60*, 22513–22521. [CrossRef]
26. Wu, Y.; Chen, X.; Han, Y.; Yue, D.; Cao, X.; Zhao, Y.; Qian, X. Highly efficient utilization of nano-Fe(0) embedded in mesoporous carbon for activation of peroxydisulfate. *Environ. Sci. Technol.* **2019**, *53*, 9081–9090. [CrossRef] [PubMed]
27. Wang, Y.; Ren, N.; Xi, J.; Liu, Y.; Kong, T.; Chen, C.; Xie, Y.; Duan, X.; Wang, S. Mechanistic investigations of the pyridinic N−Co structures in Co embedded N-doped carbon nanotubes for catalytic ozonation. *ACS EST Eng.* **2021**, *1*, 32–45. [CrossRef]
28. Fu, W.; Hu, Z.; Zheng, Y.; Su, P.; Zhang, Q.; Jiao, Y.; Zhou, M. Tuning mobility of intermediate and electron transfer to enhance electrochemical reduction of nitrate to ammonia on Cu_2O/Cu interface. *Chem. Eng. J.* **2021**, *433*, 133680. [CrossRef]
29. Ding, D.; Yang, S.; Qian, X.; Chen, L.; Cai, T. Nitrogen-doping positively whilst sulfur-doping negatively affect the catalytic activity of biochar for the degradation of organic contaminant. *Appl. Catal. B Environ.* **2020**, *263*, 118348. [CrossRef]
30. Liu, C.; Li, H.; Liu, F.; Chen, J.; Yu, Z.; Yuan, Z.; Wang, C.; Zheng, H.; Henkelman, G.; Wei, L.; et al. Intrinsic activity of metal centers in metal–nitrogen–carbon single-atom catalysts for hydrogen peroxide synthesis. *J. Am. Chem. Soc.* **2020**, *142*, 21861–21871. [CrossRef]
31. Zhang, Q.; Zhou, M.; Ren, G.; Li, Y.; Li, Y.; Du, X. Highly efficient electrosynthesis of hydrogen peroxide on a superhydrophobic three-phase interface by natural air diffusion. *Nat. Commun.* **2020**, *11*, 1731. [CrossRef] [PubMed]
32. Cao, P.; Quan, X.; Zhao, K.; Chen, S.; Yu, H.; Su, Y. High-eefficiency electrocatalysis of molecular oxygen toward hydroxyl radicals enabled by an atomically dispersed iron catalyst. *Environ. Sci. Technol.* **2020**, *54*, 12662–12672. [CrossRef] [PubMed]
33. Cao, P.; Quan, X.; Zhao, K.; Chen, S.; Yu, H.; Niu, J. Selective electrochemical H_2O_2 generation and activation on a bifunctional catalyst for heterogeneous electro-Fenton catalysis. *J. Hazard. Mater.* **2020**, *382*, 121102. [CrossRef] [PubMed]
34. Tian, Y.; Fu, W.; Wang, Q.; Tang, Y.; Zhou, M. High electron transfer rate and efficiency on Fe^0 modified by sulfidation and pre-magnetization for carbamazepine degradation by heterogeneous electro-Fenton in wide pH ranges. *Chem. Eng. J.* **2022**, *427*, 131694. [CrossRef]
35. Feng, Z.; Tian, Q.; Yang, Q.; Zhou, Y.; Zhao, H.; Zhao, G. Selectively photoelectrocatalytic reduction of oxygen to hydroxyl radical and singlet oxygen: Mechanism and validation in coal wastewater. *Appl. Catal. B Environ.* **2021**, *286*, 119908. [CrossRef]
36. Zhang, L.-S.; Jiang, X.-H.; Zhong, Z.-A.; Tian, L.; Sun, Q.; Cui, Y.-T.; Lu, X.; Zou, J.-P.; Luo, S.-L. Carbon nitride supported high-loading Fe single-atom catalyst for activation of peroxymonosulfate to generate $^1O_2$ with 100 % selectivity. *Angew. Chem. Int. Edit.* **2021**, *60*, 21751–21755. [CrossRef]
37. Zuo, S.; Jin, X.; Wang, X.; Lu, Y.; Zhu, Q.; Wang, J.; Liu, W.; Du, Y.; Wang, J. Sandwich structure stabilized atomic Fe catalyst for highly efficient Fenton-like reaction at all pH values. *Appl. Catal. B Environ.* **2021**, *282*, 119551. [CrossRef]
38. Zhao, Y.; Sun, M.; Wang, X.; Wang, C.; Lu, D.; Ma, W.; Kube, S.A.; Ma, J.; Elimelech, M. Janus electrocatalytic flow-through membrane enables highly selective singlet oxygen production. *Nat. Commun.* **2020**, *11*, 6228. [CrossRef]
39. Ramel, F.; Birtic, S.; Ginies, C.; Soubigou-Taconnat, L.; Triantaphylidès, C.; Havaux, M. Carotenoid oxidation products are stress signals that mediate gene responses to singlet oxygen in plants. *Proc. Natl. Acad. Sci. USA* **2012**, *109*, 5535–5540. [CrossRef]
40. Fan, Y.; Ji, Y.; Kong, D.; Lu, J.; Zhou, Q. Kinetic and mechanistic investigations of the degradation of sulfamethazine in heat-activated persulfate oxidation process. *J. Hazard. Mater.* **2015**, *300*, 39–47. [CrossRef]

41. Chen, C.; Liu, L.; Li, Y.; Li, W.; Zhou, L.; Lan, Y.; Li, Y. Insight into heterogeneous catalytic degradation of sulfamethazine by peroxymonosulfate activated with $CuCo_2O_4$ derived from bimetallic oxalate. *Chem. Eng. J.* **2020**, *384*, 123257. [CrossRef]
42. Ge, L.; Zhang, P.; Halsall, C.; Li, Y.; Chen, C.-E.; Li, J.; Sun, H.; Yao, Z. The importance of reactive oxygen species on the aqueous phototransformation of sulfonamide antibiotics: Kinetics, pathways, and comparisons with direct photolysis. *Water Res.* **2019**, *149*, 243–250. [CrossRef] [PubMed]
43. El Jery, A.; Aldrdery, M.; Shirode, U.R.; Gavilán, J.C.; Elkhaleefa, A.; Sillanpää, M.; Sammen, S.S.; Tizkam, H.H. An efficient investigation and machine learning-based prediction of decolorization of wastewater by using zeolite catalyst in electro-Fenton reaction. *Catalysts* **2023**, *13*, 1085. [CrossRef]
44. Adachi, A.; Ouadrhiri, F.E.; Kara, M.; El Manssouri, I.; Assouguem, A.; Almutairi, M.H.; Bayram, R.; Mohamed, H.R.H.; Peluso, I.; Eloutassi, N.; et al. Decolorization and degradation of methyl orange azo dye in aqueous solution by the electro-Fenton process: Application of optimization. *Catalysts* **2022**, *12*, 665. [CrossRef]
45. Li, T.; Ge, L.; Peng, X.; Wang, W.; Zhang, W. Enhanced degradation of sulfamethoxazole by a novel Fenton-like system with significantly reduced consumption of H_2O_2 activated by g-C_3N_4/MgO composite. *Water Res.* **2021**, *190*, 116777. [CrossRef] [PubMed]
46. Jing, J.; Pervez, M.N.; Sun, P.; Cao, C.; Li, B.; Naddeo, V.; Jin, W.; Zhao, Y. Highly efficient removal of bisphenol A by a novel Co-doped $LaFeO_3$ perovskite/PMS system in salinity water. *Sci. Total Environ.* **2021**, *801*, 149490. [CrossRef] [PubMed]
47. Wang, F.; Wu, Y.; Gao, Y.; Li, H.; Chen, Z. Effect of humic acid, oxalate and phosphate on Fenton-like oxidation of microcystin-LR by nanoscale zero-valent iron. *Sep. Purif. Technol.* **2016**, *170*, 337–343. [CrossRef]
48. Zhou, X.; Xu, D.; Chen, Y.; Hu, Y. Enhanced degradation of triclosan in heterogeneous E-Fenton process with MOF-derived hierarchical Mn/Fe@PC modified cathode. *Chem. Eng. J.* **2020**, *384*, 123324. [CrossRef]
49. Yu, F.; Wang, Y.; Ma, H.; Zhou, M. Hydrothermal synthesis of FeS_2 as a highly efficient heterogeneous electro-Fenton catalyst to degrade diclofenac via molecular oxygen effects for Fe(II)/Fe(III) cycle. *Sep. Purif. Technol.* **2020**, *248*, 117022. [CrossRef]